

Flutter of a Periodically Supported Elastic Strip in a Gas Flow with a Small Supersonic Velocity

V. V. Vedeneev* and S. V. Shitov**

*Institute of Mechanics, Lomonosov Moscow State University,
Michurinskii pr. 1, Moscow, 119192 Russia*

Received March 4, 2013

Abstract—It is assumed in all classical studies of panel flutter that the unsteady pressure of a gas flow can be calculated according to the piston theory. But the piston theory holds only for large Mach numbers and does not cover the region $1 < M < 2$. It was recently shown that, in this range of Mach numbers, there is a region of panel flutter, referred to as single-mode flutter, which differs from the “classical” (coupled) flutter. In the present paper, single-mode flutter is studied numerically for a strip-shaped periodically supported plate. The boundaries of stability are constructed, and the influence of the strip width and the distance between the supports is analyzed.

DOI: 10.3103/S0025654415030085

Keywords: *panel flutter, plate flutter, single-mode flutter, single-degree-of-freedom flutter.*

1. INTRODUCTION

Panel flutter is the phenomenon of self-excited vibrations of lining panels in aircraft moving at a large velocity. Usually, this flutter does not lead to the instantaneous fracture of the panels (in contrast to wing flutter), but it results in rapid accumulation of the fatigue damage and sharply decreases the operation life of the panels. Although panel flutter was observed in supersonic rockets already during the WWII, the first meaningful theoretical studies appeared several decades later [1, 2]. These studies were based on the use of the Kirchhoff–Love model of the plate motion and the law of plane sections for the gas pressure on the plate [3]. After Movchan’s studies, the panel flutter problem was investigated in many complicated settings [4, 10]. In an overwhelming majority of studies, the “elastic” part of the problem was sophisticated; namely, multilayer and composite plates, nonflat shells, and nonlinear models of the plate and the material including viscoelastic materials, shape memory materials, and materials with piezoelectric properties were considered [11–13]. The “aerodynamic” part of the problem remained unchanged; namely, the piston theory was used.

For the linearized unsteady pressure of an inviscid gas acting on a vibrating plate, gas dynamics provides an expression in the form of an integral operator, applied to a combination of the deflection and its derivative, with kernel containing special functions (see the statement of the problem below). This expression gives the piston theory formula in the limit as $M \rightarrow \infty$ but has nothing in common with the piston theory for Mach numbers close to unity. The substitution of the exact expression into the equation of the plate motion leads to an integro-differential equation for the eigenvalues which, because of the complexity of the mathematical problem, has been examined only in a few papers. In [14], the general solution of this integro-differential equation was obtained analytically, and the eigenvalue problem was thus reduced to an algebraic problem, but the latter turned out to be so complicated that no attempts have been made to solve it directly. In [7, 15, 16], the integro-differential equation was solved numerically by the Bubnov–Galerkin and finite element methods for some specific parameters of the problem. It was noted that, along with coupled flutter, which is obtained when the problem is solved by using the piston theory, flutter of a different type, i.e., single-mode flutter, was obtained in calculations for $1 < M < 2$. But this was explained by a numerical error, and several authors even claimed this to be a nonphysical effect.

* e-mail: vasily.vedeneev@mail.ru

** e-mail: shltov@gmail.com

Later, the problem of studying panel flutter by using nonlinear aerodynamic models was solved numerically in a number of papers. Flutter at transonic velocities was studied in [17, 18], where the Euler equations were solved, and flutter in a viscous gas was investigated in [19–22], where the Navier–Stokes equations were solved. In these studies, the problem of the plate motions in time was studied directly, and the unstable state was not divided into single-mode flutter and coupled flutter.

In [23], panel flutter for a plate shaped as a strip of large dimensions (two-dimensional problem) was studied by an asymptotic method [24]. It was rigorously proved that single-mode flutter exists, the physical vibration amplification mechanism was revealed, and it was shown that it cannot be discovered when solving the problem by the piston theory and generally by using aerodynamic models where the unsteady pressure on the plate is expressed in terms of its deflection in the form of any differential constraint. Later this problem was solved numerically [25], and the stability boundaries were constructed for the first six eigenmodes. It was also shown that the instability domain consists of a coupled flutter domain and single-mode flutter domains for various modes and that single-mode flutter significantly extends the instability domain towards the region of small Mach numbers and short plates. The influence of the boundary layer [26], as well as of the structural damping of the plate [27] was studied as well, and the limit cycles of nonlinear flutter vibrations were analyzed [28, 29]. Finally, experiments were performed [30], where single-mode flutter excitation for Mach numbers in the interval $1 < M < 1.3$ was registered for the first time. Thus, single-mode flutter of an elastic strip (two-dimensional statement of the problem) has currently been studied to a large extent.

The three-dimensional problem of single-mode panel flutter was studied in [31, 32] for rectangular plates of large dimensions by using the modified asymptotic method developed in [33]. The statement of the problem of studying the rectangular plates numerically without any additional assumptions about their dimensions is more complicated than the two-dimensional problem, because the integration domain in the integro-differential expression for the unsteady pressure acting on the plate becomes two-dimensional and has the shape of a triangle [34]. But this two-dimensional integral can be reduced to a one-dimensional integral in one special case, i.e., in the case of an infinite series of rectangular plates connected by hinges or, which is the same, in the case of a periodically supported elastic strip. This statement of the problem can be considered as the first approximation to the study of flutter of an isolated rectangular plate. In this paper, we solve this problem numerically by the modified method developed in [25].

2. STATEMENT OF THE PROBLEM

In the linear approximation, we study the stability of a thin elastic infinite strip built into an absolutely rigid plane surface. One side of the strip is in a supersonic gas flow, and the other side is subjected to constant pressure, which balances the strip in the plane unperturbed state. The strip is periodically supported by hinges along the infinite direction; its front and back edges are also hinged (see Figs. 1 and 2). Because of periodicity, all spans are either simultaneously stable or simultaneously unstable, and hence in what follows, we consider the stability of an individual span as an element of the strip directly interacting with the neighboring spans. The individual span itself will be called the plate.

We place the coordinate system $Oxyz$ in the plane of the unperturbed strip so that the plate under study occupies the domain $0 \leq x \leq L_{xw}$, $0 \leq y \leq L_{yw}$, $z = 0$. The z -axis is perpendicular to the plate plane so that the coordinate system forms a right trihedron.

We assume that there is no membrane stress in the plate, but the plate has flexural rigidity D_w , which, together with the thickness h and the material density ρ_m , is assumed to be constant. The plate vibrations are small (i.e., the plate deflection is small compared with the thickness) and are described by the Kirchhoff–Love equation of motion. The mass forces are neglected.

The gas is assumed to be inviscid and perfect with density ρ_0 and speed of sound a_0 in the unperturbed state. The gas flow is translational in the domain $z > 0$ with a constant supersonic velocity U_0 in the direction of the x -axis. The flow is assumed to be adiabatic, and the boundary layer is neglected.

We assume that a small perturbation is imposed on the plate at the initial time. Let us prove that if the gas flow incoming from infinity does not contain perturbations and the perturbations themselves are initiated by the plate, then the perturbed gas motion is potential. Indeed, the unperturbed gas motion is potential and the plate action on the gas is equivalent to the application of surface forces, which can cause only a potential flow by the Thompson theorem. Therefore, the gas perturbations due to the plate are always potential.

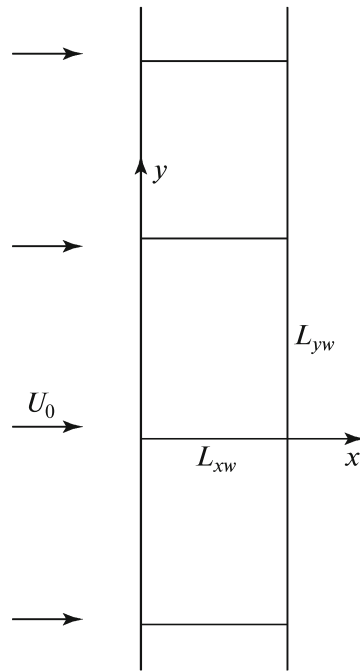


Fig. 1.

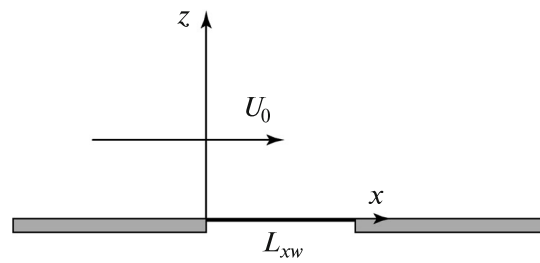


Fig. 2.

Now assume that the flow is locally perturbed as well and the perturbation contains a vortical part. By the Thompson theorem, this part is frozen in the gas particles, acts on the plate as a static load on a finite time interval, and hence cannot result in instability. Thus, it suffices to consider only potential perturbations of the gas in stability analysis.

The Kirchhoff–Love equations of a thin elastic plate motion in the gas flow and the boundary condition of hinged fixation at the plate edges have the form

$$\begin{aligned}
 \rho_m h \frac{\partial^2 w}{\partial t^2} + D_w \Delta_{xy}^2 w + p &= 0, \quad 0 < x < L_{xw}, \\
 w = \frac{\partial^2 w}{\partial x^2} &= 0, \quad x = 0, \quad L_{xw}, \\
 w = \frac{\partial^2 w}{\partial y^2} &= 0, \quad y = 0, \quad L_{yw},
 \end{aligned}
 \tag{2.1}$$

where Δ_{xy} is the two-dimensional Laplace operator and $w(x, y, t)$ is the plate deflection. It follows from the linearized theory of gas motion that the pressure difference $p(x, y, t)$ acting on the plate can be expressed in terms of the gas motion potential $\varphi(x, y, z, t)$ as

$$p(x, y, t) = -\rho_0 \left(\frac{\partial}{\partial t} + U_0 \frac{\partial}{\partial x} \right) \varphi(x, y, 0, t).
 \tag{2.2}$$

The system of linearized equations and boundary conditions describing the development of small gas perturbations has the form

$$\begin{aligned} & \left(\frac{\partial}{\partial t} + U_0 \frac{\partial}{\partial x} \right)^2 \varphi - a_0^2 \frac{\partial^2 \varphi}{\partial x^2} - a_0^2 \frac{\partial^2 \varphi}{\partial y^2} - a_0^2 \frac{\partial^2 \varphi}{\partial z^2} = 0, \quad z > 0, \\ & \left(\frac{\partial \varphi}{\partial x}, \frac{\partial \varphi}{\partial y}, \frac{\partial \varphi}{\partial z} \right) \rightarrow 0 \quad \text{as } z \rightarrow +\infty \text{ along the ray } z = \frac{x - x_0}{\sqrt{M^2 - 1}}, \\ & \frac{\partial \varphi}{\partial z} = \frac{\partial w}{\partial t} + U_0 \frac{\partial w}{\partial x}, \quad z = 0, \quad x \in [0, L_{xw}]; \quad \frac{\partial \varphi}{\partial z} = 0, \quad z = 0, \quad x \notin [0, L_{xw}]. \end{aligned} \tag{2.3}$$

The first equation in the system is the wave equation, where a_0 is the speed of sound in the gas. The second condition that $\text{grad } \varphi$ tends to zero as $z \rightarrow +\infty$ along the characteristic $z = (x - x_0)/\sqrt{M^2 - 1}$ for fixed t and y holds only for perturbations whose are generated near the plate and increase with time. Indeed, if we fix the coordinates y and t and increase z along the characteristic, then we observe the perturbations generated at the preceding time instants, and since the perturbation increase, they decay if time is counted backwards. The third condition in (2.3) is the gas flow tangency condition on the vibrating plate and the surrounding absolutely rigid plane.

To pass to dimensionless variables, we take $a_0, \rho_0,$ and h as dimension-independent quantities. Then we have (the dimensionless variables are denoted by tilde)

$$x = \tilde{x}h, \quad y = \tilde{y}h, \quad z = \tilde{z}h, \quad t = \frac{\tilde{t}h}{a_0}, \quad \varphi = \tilde{\varphi}a_0h, \quad w = \tilde{w}h.$$

In what follows, the tildes over the symbols are omitted for brevity, and all variables are assumed to be dimensionless.

The dimensionless parameters are expressed in terms of the dimensional ones as follows:

$$D = \frac{D_w}{a_0^2 \rho_m h^3}, \quad L_x = \frac{L_{xw}}{h}, \quad L_y = \frac{L_{yw}}{h}, \quad M = \frac{U_0}{a_0}, \quad \mu = \frac{\rho_0}{\rho_m}.$$

Here $D, L_x,$ and L_y are the dimensionless rigidity, length, and width of the plate, and M and μ are the Mach number and the dimensionless gas density.

The stability of an elastic plate in the gas flow is determined by the behavior of eigenmodes, and therefore we further assume that the small perturbations of the plate and gas have the form

$$\begin{aligned} w(x, y, t) &= W(x, y)e^{-i\omega t}, \\ \varphi(x, y, z, t) &= \Phi(x, y, z)e^{-i\omega t}. \end{aligned} \tag{2.4}$$

With expressions (2.4) and the procedure of passing to dimensionless variables taken into account, the closed system of dimensionless equations for perturbations consists of the plate motion equations

$$\begin{aligned} D\Delta_{xy}^2 W - \omega^2 W + P &= 0, \quad 0 < x < L, \\ P &= -\mu \left(-i\omega + M \frac{\partial}{\partial x} \right) \Phi(x, y, 0), \\ W &= 0, \quad x < 0, \quad x > L_x, \\ W &= \frac{\partial^2 W}{\partial x^2} = 0, \quad x = 0, \quad x = L_x, \\ W &= \frac{\partial^2 W}{\partial y^2} = 0, \quad y = 0, \quad y = L_y \end{aligned} \tag{2.5}$$

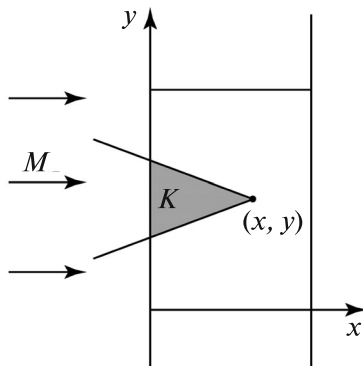


Fig. 3.

and the gas motion equations

$$\begin{aligned} \left(-i\omega + M \frac{\partial}{\partial x}\right)^2 \Phi - \frac{\partial^2 \Phi}{\partial x^2} - \frac{\partial^2 \Phi}{\partial y^2} - \frac{\partial^2 \Phi}{\partial z^2} &= 0, \quad z > 0, \\ \left(\frac{\partial \varphi}{\partial x}, \frac{\partial \varphi}{\partial y}, \frac{\partial \varphi}{\partial z}\right) &\rightarrow 0 \quad \text{as } z \rightarrow +\infty \text{ along the ray } z = \frac{x - x_0}{\sqrt{M^2 - 1}}, \\ \frac{\partial \Phi}{\partial z} &= -i\omega W + M \frac{\partial W}{\partial x}, \quad z = 0. \end{aligned} \quad (2.6)$$

Equation (2.6) for the potential Φ can be solved analytically by using the Laplace transform [34, §4.8], and its solution has the form

$$\begin{aligned} \Phi(x, y, 0) &= \iint_K -\frac{1}{\pi} \left[-i\omega W(x_1, y_1) + M \frac{\partial W(x_1, y_1)}{\partial x_1} \right] \exp \left[\frac{i\omega M}{\beta^2} (x - x_1) \right] \\ &\quad \times \frac{1}{\sqrt{(x - x_1)^2 - \beta^2 y_1^2}} \cos \left[\frac{\omega}{\beta^2} \sqrt{(x - x_1)^2 - \beta^2 y_1^2} \right] dx_1 dy_1, \end{aligned} \quad (2.7)$$

where K is the triangle obtained by the intersection of the inverted Mach cone issuing from the point (x, y) with the entire plate (Fig. 3) and $\beta = \sqrt{M^2 - 1}$.

Thus, after substitution of the expression (2.7) into the plate motion equation (2.5), this equation with the boundary conditions of hinged support is the problem of determining the complex eigenvalues ω . This problem is solved numerically. We note that the eigenvalue ω enters the equation in a complex way; such problems were studied in several papers (e.g., see [35]). The system is unstable if and only if at least one of the eigenfrequencies ω_n lies in the upper half-plane $\text{Im } \omega_n > 0$ of the complex plane. The aim of the paper is to construct the instability domains in the space of dimensionless parameters of the problem.

3. NUMERICAL METHOD

We solve the eigenvalue problem for the integro-differential equation (2.5) of the plate motion with the expression (2.7) for the potential Φ taken into account numerically by the Bubnov–Galerkin method. The method developed on the basis of [25] will be described below.

The plate deflection $W(x, y)$ is represented as the superposition of basis functions for which we take the mode shapes of the plate vibrations in vacuum,

$$W(x, y) = \sum_{k=1}^{N_x} \sum_{l=1}^{N_y} C_l^k \sin \frac{k\pi x}{L_x} \sin \frac{l\pi y}{L_y} = \sum_{k=1}^{N_x} \sum_{l=1}^{N_y} C_l^k W_k(x) W^l(y), \quad (3.1)$$

where the C_l^k are unknown constant coefficients. The basis functions can be represented as $N_x \times N_y$ tables (see Table 1) so that the column number is the number of the basis function with respect to x and the row number is the number of the basis function with respect to y .

Table 1

	1	2	3	...	N_x
1	$W_1(x)W^1(y)$	$W_2(x)W^1(y)$	$W_3(x)W^1(y)$...	$W_{N_x}(x)W^1(y)$
2	$W_1(x)W^2(y)$	$W_2(x)W^2(y)$	$W_3(x)W^2(y)$...	$W_{N_x}(x)W^2(y)$
3
...
N_y	$W_1(x)W^{N_y}(y)$	$W_2(x)W^{N_y}(y)$	$W_3(x)W^{N_y}(y)$...	$W_{N_x}(x)W^{N_y}(y)$

We number them as follows:

$$T_{(l-1)N_x+k}(x, y) = W_k(x)W^l(y).$$

The sum (3.1) can be rewritten as

$$W(x, y) = \sum_{m=1}^N C_m T_m(x, y), \quad T_m(x, y) = W_k(x)W^l(y), \quad C_m = C_l^k, \quad (3.2)$$

where $N = N_x N_y$. The numbers k and l can be reconstructed from the number m ,

$$l = \left[\frac{m-1}{N_x} \right] + 1, \quad k = m - N_x(l-1), \quad (3.3)$$

where the square brackets denote the integer part. Further, we substitute the sum (3.2) into the plate motion equation (2.5). We multiply it successively by $(2/L_y)T_n(x, y)$, $n = 1, \dots, N$, integrate over x from 0 to L_x and over y from 0 to L_y , and obtain a homogeneous system of linear algebraic equations for the complex coefficients C_m with matrix $A(\omega)$,

$$A(\omega) = K - \frac{L_x \omega^2}{2} E + P(\omega). \quad (3.4)$$

Here E is the identity matrix and K is the diagonal rigidity matrix responsible for the properties of the plate. Its entries k_{mm} have the form

$$k_{mm} = \frac{L_x}{2} D \left[\left(\frac{k\pi}{L_x} \right)^4 + 2 \left(\frac{k\pi}{L_x} \right)^2 \left(\frac{l\pi}{L_y} \right)^2 + \left(\frac{l\pi}{L_y} \right)^4 \right],$$

where the indices k and l are calculated in terms of m by formula (3.3) and P is the matrix of aerodynamic forces with entries

$$p_{nm}(\omega) = \frac{2}{L_y} \int_0^{L_y} \int_0^{L_x} P(x, y, T_m, \omega) T_n(x, y) dx dy. \quad (3.5)$$

In Section 5, we transform the expression (3.5) and describe a method for calculating the entries of the matrix P .

Thus, the equation for the eigenfrequencies has the form

$$\det A(\omega) = 0 \quad \Leftrightarrow \quad \det \left(K - \frac{L_x \omega^2}{2} E + P(\omega) \right) = 0. \quad (3.6)$$

4. METHOD FOR SOLVING THE FREQUENCY EQUATION

Consider the plate in a vacuum. This case is described by the frequency equation (3.6) without the matrix P responsible for the presence of aerodynamic forces,

$$\det \left(K - \frac{L_x \omega^2}{2} E \right) = 0. \quad (4.1)$$

This equation has N distinct real solutions for ω^2 , which are associated with the frequencies $\omega_{n0} = \sqrt{(2/L_x)k_{nn}}$ in vacuum. We do not consider the negative frequencies, because the corresponding eigenmotions coincide for negative and positive frequencies.

If the aerodynamic forces are added, then the frequencies cease to be real. This follows from the fact that the matrix $P(\omega)$ is nonsymmetric and complex. Therefore, the eigenvalue problem is not self-adjoint, and the eigenfrequencies are complex.

We solve the frequency equation numerically by using two modifications of the iteration method. First, it is necessary to calculate the n th eigenfrequency ω_n . For the initial approximation we take the n th eigenfrequency $\omega_{n0} = \sqrt{(2/L_x)k_{nn}}$ in vacuum. Further, we assume that the p th approximation ω_{np} is known. We compose the matrix $A_{p+1}(\omega_{np}, \omega_{n(p+1)})$ so that $\omega_{n(p+1)}$ is contained in this matrix in the simplest way. We choose all its entries a_{ij} except for a_{nn} so that they are the same as in the matrix $A(\omega_{np})$ and calculate the coefficient a_{nn} by the formula

$$a_{nn} = k_{nn} - \frac{L_x}{2}(\omega_{n(p+1)})^2 + p_{nn}(\omega_{np}), \quad (4.2)$$

where k_{nn} and p_{nn} are the corresponding entries of the matrices K and P .

Thus, the equation for the $(p+1)$ st approximation $\omega_{n(p+1)}$ has the form

$$\det[A_{p+1}(\omega_{np}, \omega_{n(p+1)})] = 0. \quad (4.3)$$

This is a linear equation for $(\omega_{n(p+1)})^2$, and in the set of these two values, we take $\omega_{n(p+1)}$ in the right half-plane of the complex plane $\text{Re } \omega_{n(p+1)} > 0$.

We continue to calculate the iterations of ω_n until the following condition is satisfied:

$$\left| \frac{\omega_{np} - \omega_{n(p-1)}}{\omega_{np}} \right| < \varepsilon. \quad (4.4)$$

The calculations were performed for $\varepsilon = 10^{-6}$. The convergence problem will be considered in Section 6.

The second modification of the iteration method is used in the case of frequencies $\omega_n = \omega_1^j$ and $\omega_{n+1} = \omega_2^j$ (here we use the notation $\omega_n = \omega_l^k$ as in the case of basis functions), which are responsible for the appearance of coupled flutter. This method is based on the fact that, for certain parameters of the problem, these two frequencies approach each other in the complex plane. It is necessary to use the modified iteration method, because the iterations may be cycled as they approach the desired frequency, so that $\omega_{n(p+1)}$ jumps from one branch to the other. The modified method solves this problem as follows. We compose the matrix $A_{p+1}(\omega_{np}, \omega_{n(p+1)})$ for the following approximation, which simultaneously contains two entries of the matrix

$$a_{jj} = k_{jj} - \frac{L_x}{2}(\omega_{n(p+1)})^2 + p_{jj}(\omega_{np}), \quad j = n, n+1. \quad (4.5)$$

All other coefficients a_{ij} of the matrix $A_{p+1}(\omega_{np}, \omega_{n(p+1)})$ remain the same as $A(\omega_{np})$. By solving the equation $\det A_{p+1}(\omega_{np}, \omega_{n(p+1)}) = 0$, we obtain four roots and take two of them with positive real part, s_1 and s_2 . These two roots correspond to the two frequencies ω_n and ω_{n+1} . The following criterion allows us to choose the root corresponding to the desired frequency correctly. We let s_3 denote the point at the middle of the segment connecting s_1 and s_2 in the complex plane $s_3 = \frac{1}{2}(s_1 + s_2)$. We draw the straight line through s_3 at the angle $\pi/4$ to the real axis. The root above this straight line corresponds to the frequency ω_n , and the other root corresponds to the frequency ω_{n+1} . Thus, if $(\text{Im } s_1 - \text{Im } s_3) > (\text{Re } s_1 - \text{Re } s_3)$, then $s_1 = \omega_n$ and $s_2 = \omega_{n+1}$, and vice versa.

5. CALCULATION OF THE AERODYNAMIC MATRIX P

To calculate the entries of the aerodynamic matrix $P(\omega)$, it is necessary to calculate the perturbation of the pressure P which enters the equation of motion (2.5). Formula (2.7) is the analytic expression

of the potential $\Phi(x, y, \omega)$. Let us transform it for $W(x, y) = \sin(\kappa x) \sin(\lambda y)$. We represent the two-dimensional integral over the triangle K as a repeated integral over x and y ; then the integral over y can be calculated analytically. The obtained expression has the form

$$\Phi(x, y) = -\frac{1}{\beta} \sin(\lambda y) \int_0^x (-i\omega \sin(\kappa x_1) + M\kappa \cos(\kappa x_1)) \exp\left(\frac{i\omega M}{\beta^2}(x - x_1)\right) J_0(\xi) dx_1, \quad (5.1)$$

where J_0 is the Bessel function of order zero and $\xi = \sqrt{\omega^2 + (\beta\lambda)^2}(x - x_1)/\beta^2$.

Now we substitute (5.1) into the expression (2.5) for the pressure perturbation, differentiate, collect equal terms, and obtain

$$\begin{aligned} P(x, y, T_m, \omega) &= \sin(\lambda y) \left\{ \frac{\mu M}{\beta} (-i\omega \sin(\kappa x) + M\kappa \cos(\kappa x)) \right. \\ &+ \left. \frac{\mu}{\beta^3} \int_0^x (-i\omega \sin(\kappa x_1) + M\kappa \cos(\kappa x_1)) \exp\left(\frac{i\omega M}{\beta^2}(x - x_1)\right) (i\omega J_0(\xi) - M\sqrt{\omega^2 + (\lambda\beta)^2} J_1(\xi)) dx_1 \right\} \\ &= W^l(y) P_x(x, W_k, \omega). \end{aligned} \quad (5.2)$$

We use the expression (5.2) to transform formula (3.5) for the entries of the matrix P . To be definite, we set $T_m(x, y) = W_k(x)W^l(y)$ and $T_n(x, y) = W_r(x)W^s(y)$. After the substitution of (5.2) into (3.5), the two-dimensional integral splits into a repeated integral, and the integral over y can be calculated analytically,

$$\begin{aligned} p_{nm}(\omega) &= \frac{2}{L_y} \int_0^{L_y} \int_0^{L_x} P(x, y, T_m, \omega) T_n(x, y) dx dy = \frac{2}{L_y} \int_0^{L_y} \int_0^{L_x} W^l(y) P_x(x, W_k(x), \omega) W_r(x) W^s(y) dx dy \\ &= \frac{2}{L_y} \int_0^{L_y} W^l(y) W^s(y) dy \int_0^{L_x} P_x(x, W_k(y), \omega) W_r(x) dx = \delta_s^l \int_0^{L_x} P_x(x, W_k(y), \omega) W_r(x) dx, \end{aligned} \quad (5.3)$$

where δ_s^l is the Kronecker delta.

One can see that the nonzero entries p_{nm} are given by the expression $s = l$, which holds if and only if $[(m - 1)/N_x] = [(n - 1)/N_x]$. Thus, the nonzero entries p_{nm} fill square blocks on the main diagonal of the matrix P .

Further, to calculate the nonzero p_{nm} , it is required to calculate two integrals, the outer integral (5.3) and the inner integral (5.2). Both integrals are calculated by the trapezium method. The number of partition points used to calculate the outer integral was equal to $10N_x$, i.e., 10 points per half-wave of deflection of the basis function with the maximum number in the direction of the x -axis. The number of partition points used to calculate the inner integral was equal to 22. The sufficiency of this amount is studied below in Section 6.

Note that, in the flow, the mode shapes of the plate vibrations along the x -axis (the downstream direction) are different from the mode shapes of vibrations in vacuum, while the vibrations along the y -axis (the direction across the stream) do not change and are sinusoidal as in vacuum,

$$\omega_i^j(D, \mu, L_x, L_y) = \omega_i^1(D, \mu, L_x, L_y/j). \quad (5.4)$$

Thus, the boundaries of the instability domain for the frequency with number $j > 1$ coincide with the boundaries of the instability domain for the frequency with number $j = 1$ for an appropriate variation in L_y . One can readily see that, for the same reason, it suffices to set $N_y = 1$ in the calculations.

6. CONVERGENCE

Figure 4 illustrates the convergence of the four frequencies $\omega_1^1, \omega_2^1, \omega_3^1, \text{ and } \omega_4^1$ with respect to the number of basis functions N_x . The calculations were performed for $L_y = 1000$ (long-dashed lines), $L_y = 500$ (solid lines), and $L_y = 200$ (short-dashed lines) and the other dimensionless parameters were

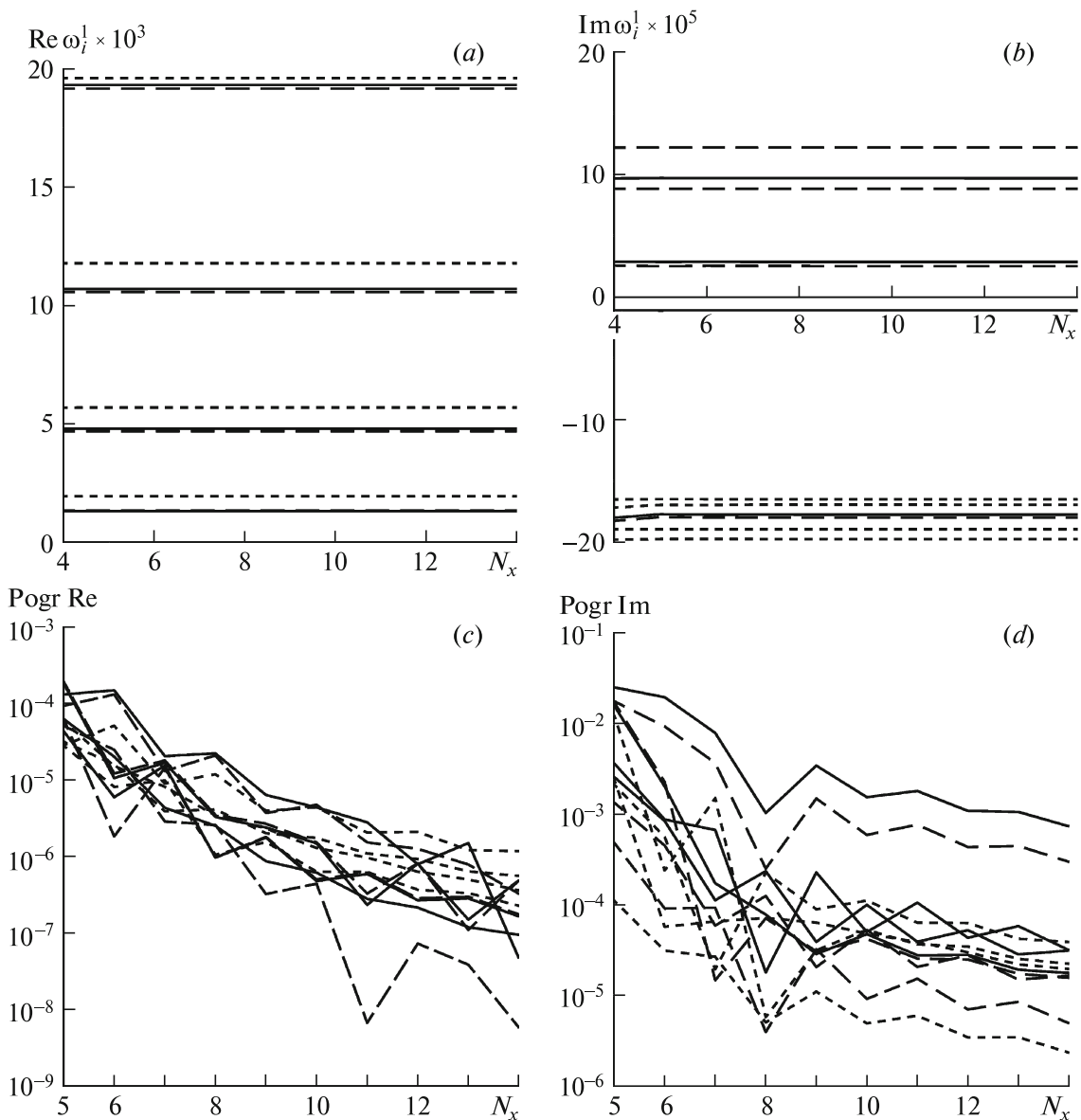


Fig. 4.

fixed: $D = 23.9$, $\mu = 0.00012$, $M = 1.2$, and $L_x = 200$. The parameter ε was set equal to 10^{-6} , the number of partition points for the outer integral was equal to $10N_x$, and the number of points for the inner integral was equal to 30. In Fig. 4 *a*, the ordinate is the real part of the frequency, and the abscissa is the number of basis functions N_x . Figure 4 *c* illustrates the relative errors of real parts corresponding to the graph in Fig. 4, *a*, which can be calculated as

$$\text{Pogr Re}(N_x) = \left| \frac{\text{Re } \omega(N_x) - \text{Re } \omega(N_x - 1)}{\text{Re } \omega(N_x)} \right|. \tag{6.1}$$

In a similar way, Figs. 4 *b*, *d* show the relative errors of imaginary parts of the same frequencies. One can see that the calculation accuracy is sufficient already for $N_x = 4$. It is this number of basis functions that was used in all subsequent calculations.

Figure 5 illustrates the convergence of the real and imaginary parts of the same four frequencies with respect to the parameter ε (4.4). All calculations were performed for the same dimensionless parameters as in Fig. 4. In Figs. 5 *a*, *b*, the ordinate is the value of the respective real or imaginary part, and the abscissa is the value of $|\log \varepsilon|$. In this case, the parameter itself is equal to 10^{-3} , 10^{-4} , 10^{-5} , 10^{-6} , 10^{-7} ,

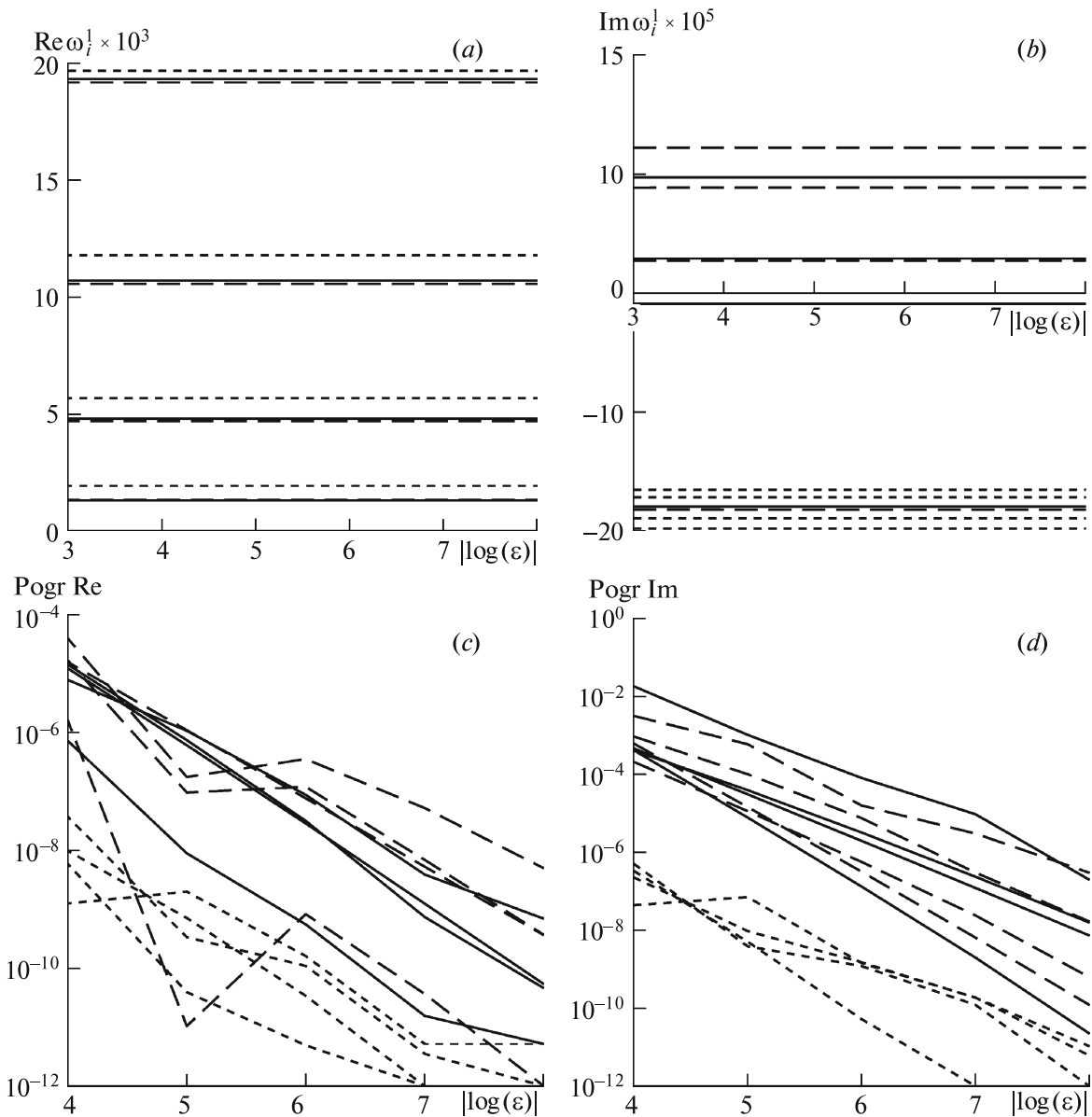


Fig. 5.

10^{-8} , respectively. Figures 5 *c, d* show the relative errors of the respective real and imaginary parts, which are calculated by analogy with (6.1). In all subsequent calculations, we set $\varepsilon = 10^{-6}$, which gives a quite satisfactory accuracy.

Consider the convergence with respect to the number of points of integration of the outer integral, Figure 6 illustrates the dependence of the frequency ω_2^1 on the number of points k_1 per one half-wave of the basis function with maximum number in the downstream direction for the partition of the inner integral (5.3). The total number of partition points for the outer integral is equal to $k_1 \cdot N_x$. In Figs. 6 *a, b*, the ordinate is the value of the respective real and imaginary parts, and Figs. 6 *c, d* show the relative errors of the real and imaginary parts calculated by analogy with (6.1). The dimensionless parameters are the same as on the preceding graphs, the values for $L_y = 1000$ are shown by dashed lines, and the values for $L_y = 500$ are shown by solid lines. In all subsequent calculations, the number of points k_1 per one half-wave is equal to 10, and the sufficiency of this number follows from the presented graphs.

Further, Fig. 7 illustrates the convergence of the real and imaginary parts of the frequency ω_2^1 with respect to the number of partition points for the inner integral (5.2). The number of points is denoted

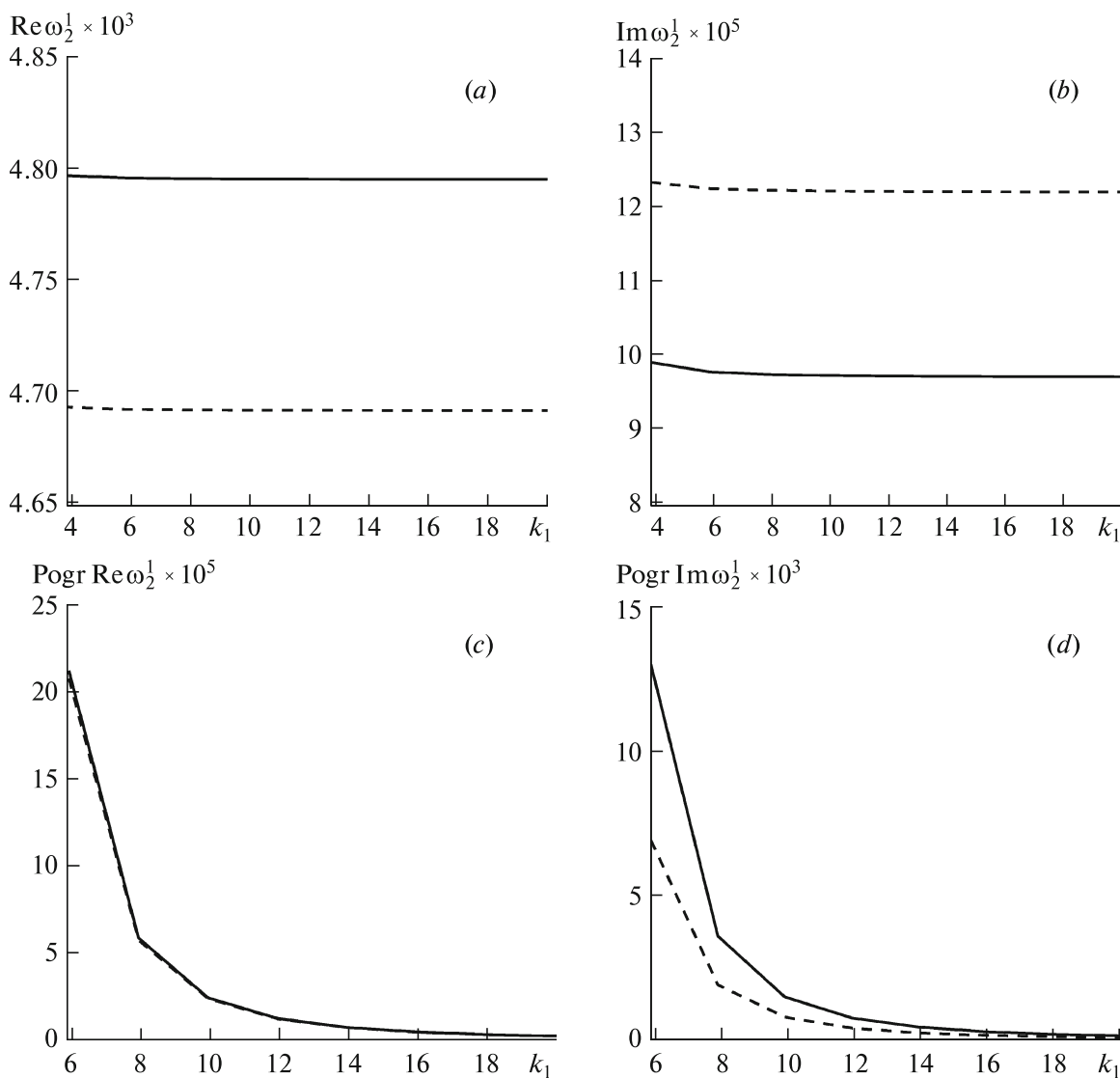


Fig. 6.

by k_2 . In all subsequent calculations, the number of partition points for the inner integral is set equal to 22.

To illustrate the iteration process, Figs. 8 *a, b* show the convergence for the frequency ω_2^1 for $L_y = 1000$ (dashed lines) and $L_y = 500$ (solid lines). The frequency in vacuum corresponds to the zero-order iteration. The calculations were performed for the same dimensionless parameters as in the preceding graphs. Figure 8 *c* shows how the value of $|\det A(\omega_2^1(p))|$ increases with the iteration number. It should be noted that, in the calculations, the iterations stop under condition (4.4), but an additional criterion for the convergence of this method is that the real and imaginary parts of the frequency tend to constant values as the number of iterations increases. This can be observed visually in Fig. 8. In a similar way, the convergence was also verified for other k frequencies for different values of the dimensionless parameters.

Thus, analyzing how the frequency convergence depends on various parameters of the numerical method, we obtained the following parameter values: $N_x = 4$, $N_y = 1$, $\varepsilon = 10^{-6}$, the number of partition points for the outer integral is $10N_x (= 40)$, and the number of partition points for the inner integral is 22. These values are used below to construct the instability domain.

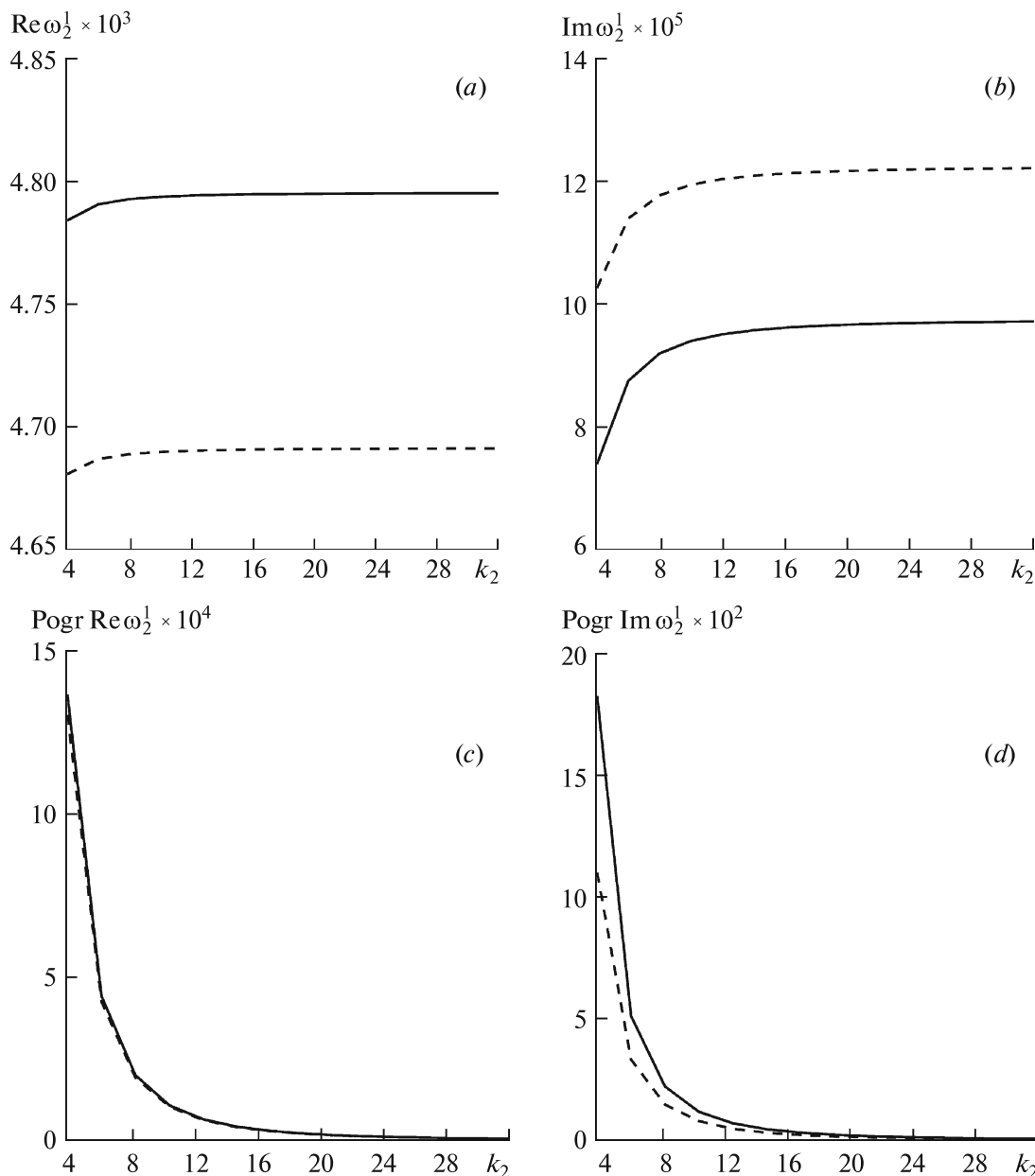


Fig. 7.

7. RESULTS

For the four eigenfrequencies ω_j^1 ($j = 1, \dots, 4$), Figs. 9 *a, b* (ω_1^1 and ω_2^1 , respectively) and Figs. 10 *a, b* (ω_3^1 and ω_4^1 , respectively) show the boundaries of the instability domain in the plane $L_x - M$, i.e., the level lines $\text{Im } \omega_j^1 = 0$. In all figures, the stability domain lies to the left, i.e., in the region of small L_x . All calculations were performed for the constant parameters of the problem $D = 23.9$ and $\mu = 0.00012$ corresponding to the case of a steel plate in air flow at the height 3000 m above sea level (or an aluminum plate in more rarefied layers).

In Fig. 9 *a*, thin lines show the boundaries of the instability domain with respect to the first mode (the frequency ω_1^1) for $L_y = 1000, 500, 450, 426, 400, 350$ (the solid and dashed boundaries alternate as L_y decreases). The domain $M < 1.5$ is shown. The maximum value of the length $L_{x \text{ max}}$ at which the plate is stable for any width L_y is 57 and corresponds to $L_y = 1000$. For $L_x > L_{x \text{ max}}$ and sufficiently large values of L_y , there is an interval $M^*(L_x, L_y) < M < M^{**}(L_x, L_y)$ where the plate is unstable with

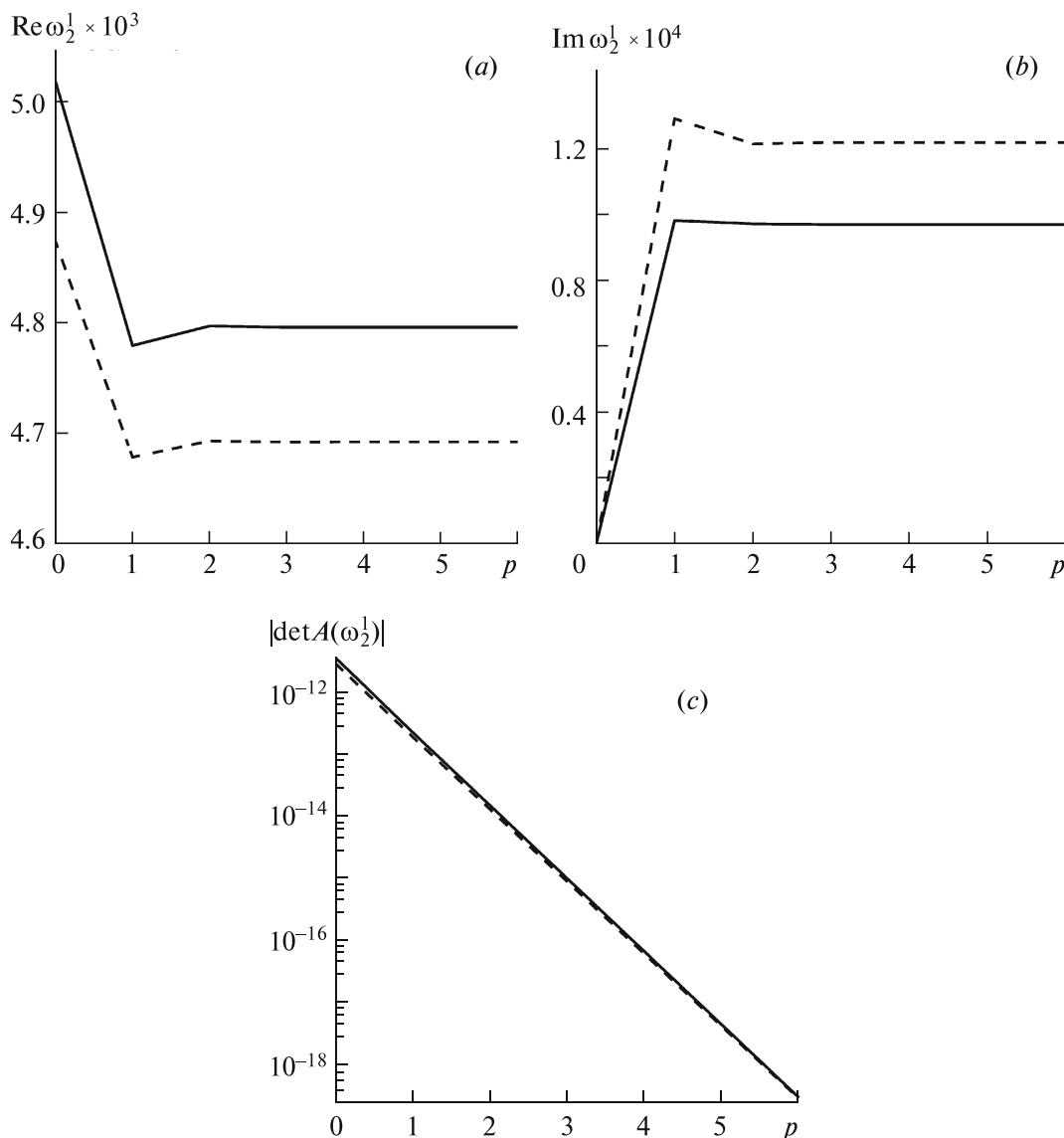


Fig. 8.

respect to the first mode. We note that the stability boundary for $L_y = 1000$ practically coincides with the boundary calculated in [25] in the two-dimensional setting, i.e., for $L_y = \infty$. As the span width L_y decreases, the range of Mach numbers at which the plate is unstable decreases and, for $L_y \approx 425$, the instability domain spits into two isolated subdomains; one of them, lying in the region of smaller values of L_x , corresponds to single-mode flutter and the other corresponds to coupled flutter. As L_y continues to decrease, the single-mode flutter domain decreases and shrinks to the values $L_x \approx 90$ and $M \approx 1.23$. For $L_y = 315$, it completely shrinks to this point and disappears. As L_y decreases, the boundary of the coupled flutter domain varies significantly slower and moves towards the region of greater values of L_x .

The bold lines in Fig. 9a show the boundaries of the stability domain calculated by the piston theory method, which can be used if the integral term in (5.2) is omitted. One can see that if the piston theory is used, then the single-mode flutter domain is completely absent and the coupled flutter boundaries calculated by the exact and piston theories closely approach each other as L_y decreases.

Figure 11 shows the flutter boundary in the range $1.5 < M < 5.0$ (the stability domain is to the left) for the same values of L_y ; the results of calculations by the exact and piston theories are shown by solid and dashed lines, respectively. One can see that single-mode flutter is absent in this range of Mach numbers and the the coupled flutter boundaries calculated by the exact and piston theories practically coincide.

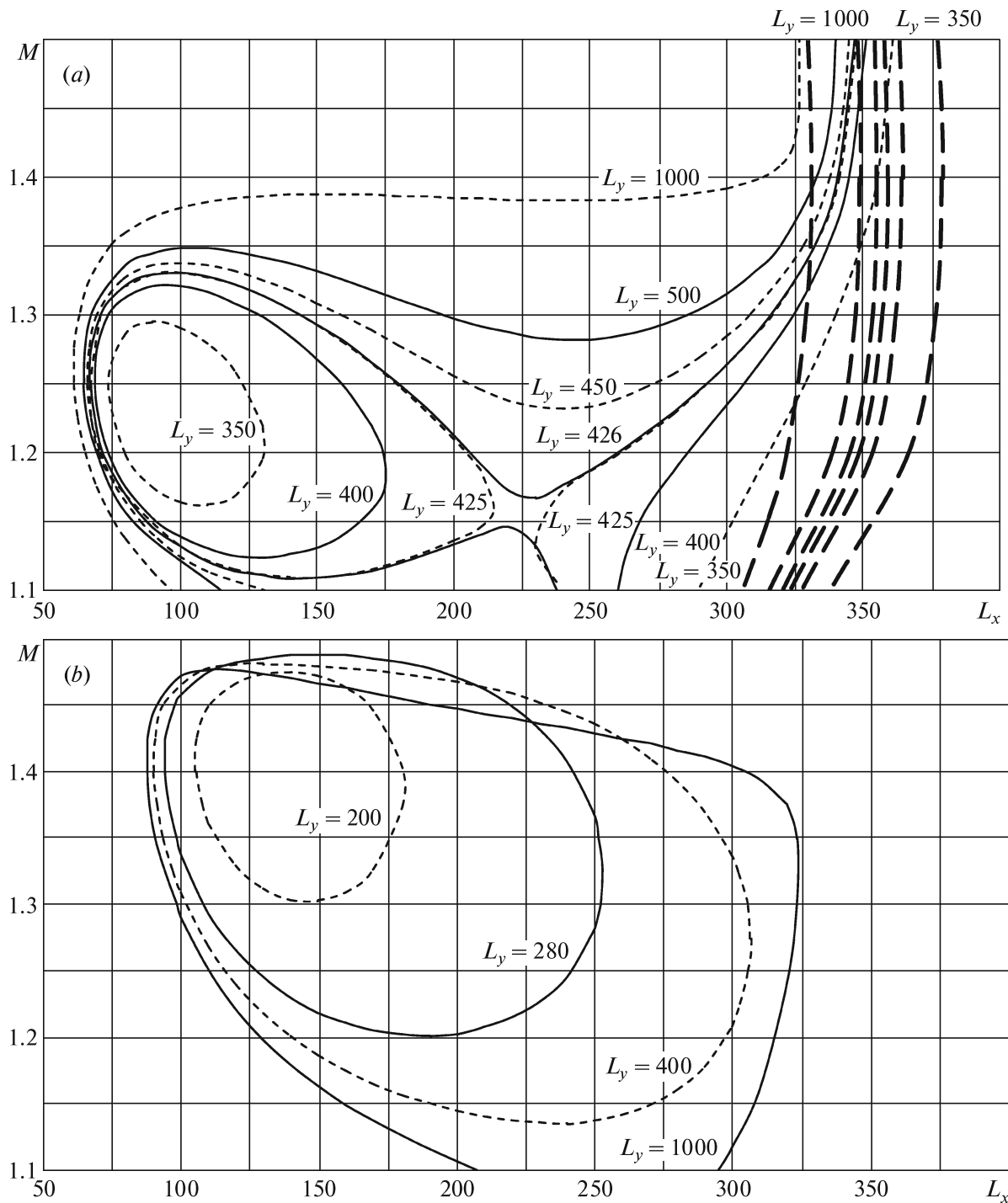


Fig. 9.

To compare the obtained results with the solution obtained by Movchan, we consider the flutter boundary given by formula (3.8) in [2], which, in the dimensionless variables used in the present paper, becomes

$$M = \frac{D}{\mu L_x^3} \frac{8\pi^3}{3\sqrt{3}} \left(5 + \left(\frac{L_x}{L_y} \right)^2 \right) \sqrt{2 + \left(\frac{L_x}{L_y} \right)^2}. \quad (7.1)$$

Compared with the version developed in [2], the version of the piston theory which is more suitable

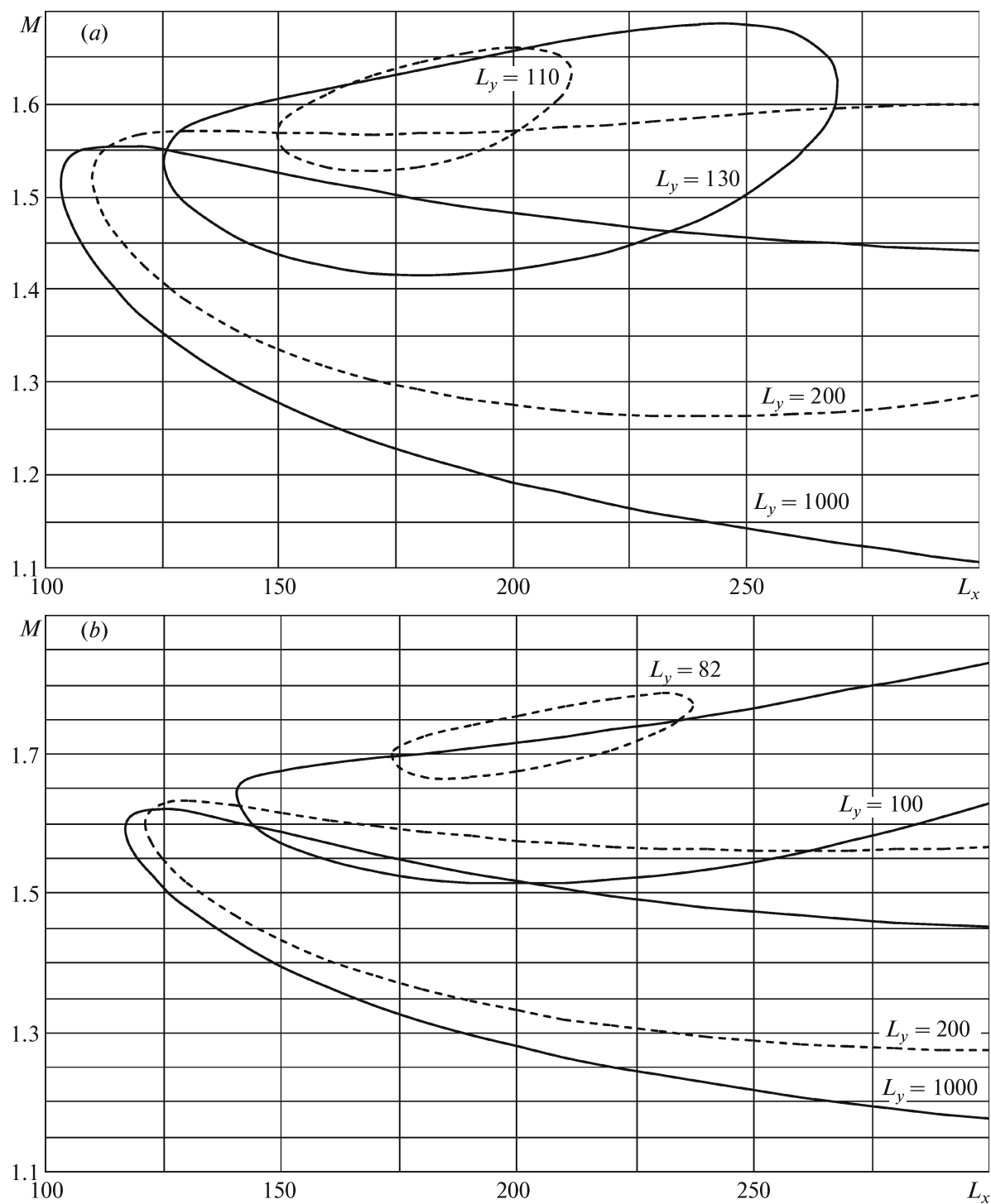


Fig. 10.

for $M < 3$ has the factor $M/\sqrt{M^2 - 1}$, where M is the Mach number. The stability boundary for this correction can be obtained from (7.1) with M on the left-hand side replaced by $M^2/\sqrt{M^2 - 1}$. In Fig. 12, the dash-dotted and dotted lines illustrate the results of the flutter boundary calculations by the original and corrected formula (7.1). In the same figure, the dashed and solid lines illustrate the results of calculations by the above-described method using the piston and exact theories. The calculations were performed for $L_y = 350, 1000$. One can see that for large Mach numbers all four methods give practically coinciding flutter boundary. For $M < 3$, the uncorrected version of the piston theory, which

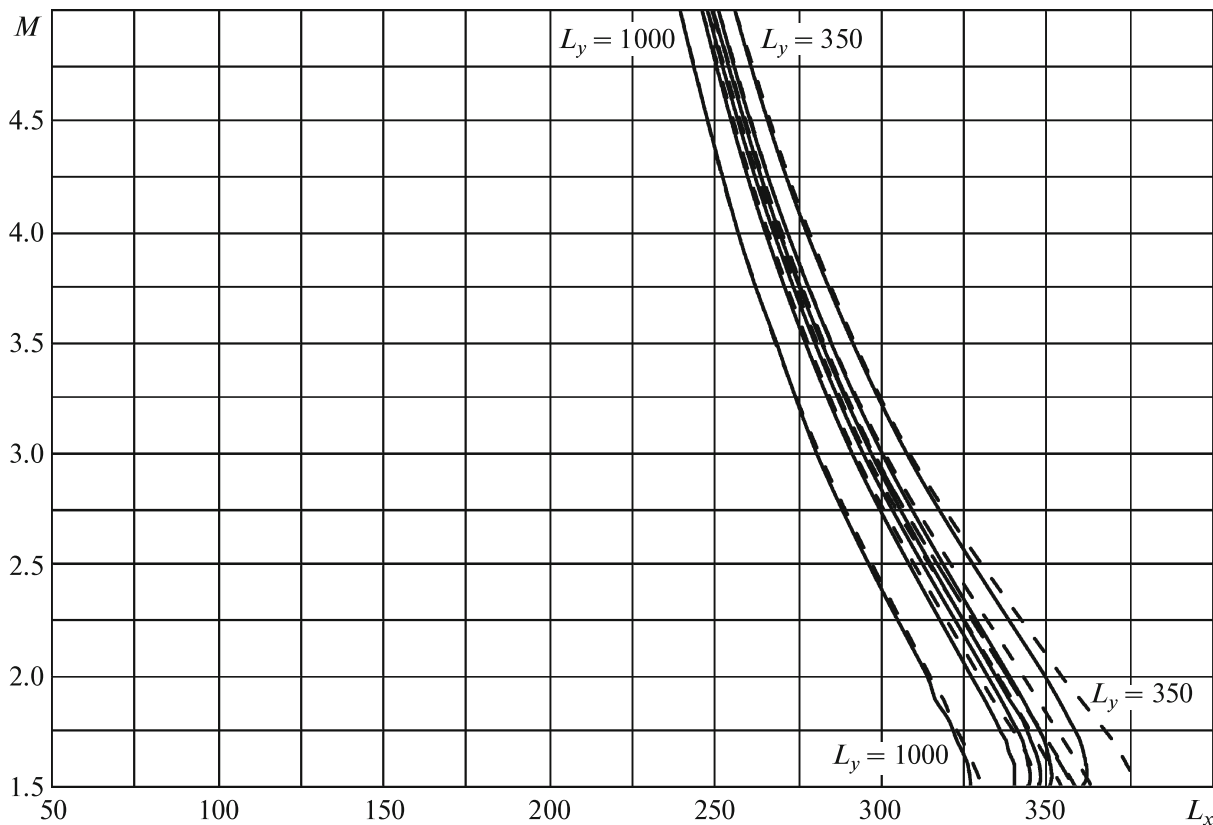


Fig. 11.

was used in [2], gives a significant error. At the same time, the corrected version remains satisfactory up to $M \approx 1.6$. For lower values of M , the piston theory is inapplicable, because it cannot reveal single-mode flutter.

Now let us analyze the stability boundaries for higher modes. Figure 9 *b* shows the flutter domain with respect to the second mode (the frequency ω_2^1) for $L_y = 1000, 400, 280, 200$. These domains are bounded on the right by the values of L_x at which coupled flutter arises, because the first and second modes get “tied up” at these values, and the first mode begins to increase while the second mode decreases. As to the first mode, a decrease in L_y results in the contraction of the single-mode flutter domain; for $L_y \approx 177$, it shrinks to the point $L_x \approx 140, M \approx 1.4$ and disappears.

In contrast to the first two modes, the boundaries of the flutter domain with respect to the third and fourth modes (which do not participate in formation of coupled flutter) respectively shown in Figs. 10 *a, b* have the asymptotes $M^* = 1$ and $M^{**} = \sqrt{2}$ as $L_x \rightarrow \infty$ for $L_y = \infty$ [25]. The boundaries for $L_y = 1000$ are very close to the results of calculation of the two-dimensional problem. As L_y decreases, the flutter domains move towards the regions of higher M and become bounded on the axis L_x . Further, as in the case of single-mode flutter with respect to the first two modes, the instability boundaries contract to a point and disappear. At the frequency ω_3^1 , the instability domain shrinks to the point $L_x \approx 190, M \approx 1.6$ and disappears for $L_y \approx 106$. In a similar way, at the frequency ω_4^1 , the instability domain shrinks to the point $L_x \approx 210, M \approx 1.73$ and disappears for $L_y \approx 81$.

The shift of the single-mode flutter domains towards the region of higher Mach numbers with decreasing L_y can be explained by the asymptotic theory of single-mode flutter [31], where under the assumption that the plate dimensions L_x, L_y are sufficiently large, the eigenmotions were represented as cyclic reflections of the waves traveling along the plate [33]. A criterion for the eigenmode amplification (i.e., the flutter criterion for a given mode) is determined by the angle between the direction of the traveling wave motion and the gas flow direction. A decrease in L_y leads to an increase in the angle between the wave and the flow and accordingly to an increase in the range of M where amplification can occur. In quantitative form, the results obtained in [31] imply the following single-mode flutter

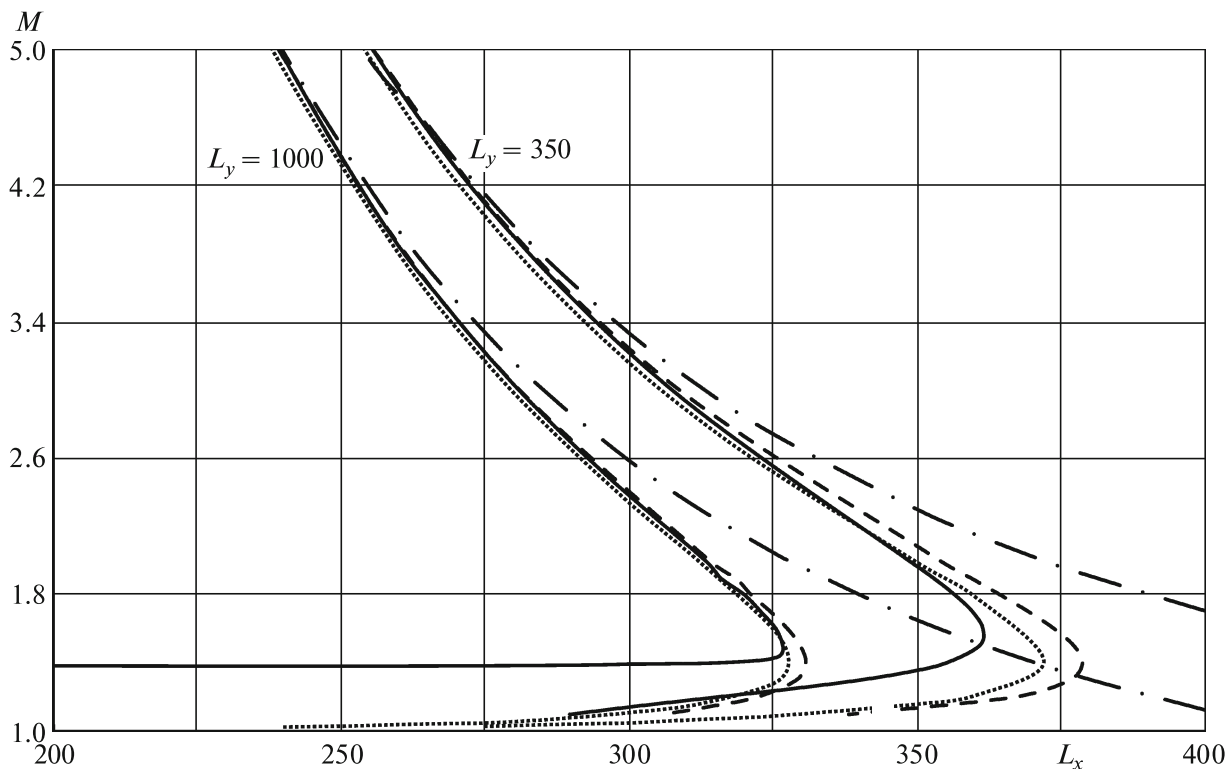


Fig. 12.

boundaries $M^*(L_x, L_y) < M < M^{**}(L_x, L_y)$:

$$\begin{aligned}
 M^* &= \sqrt{1 + \left(\frac{n}{m}\right)^2 \left(\frac{L_x}{L_y}\right)^2} (1 + \sqrt{Dk_0^2}), \\
 M^{**} &= \sqrt{1 + \left(\frac{n}{m}\right)^2 \left(\frac{L_x}{L_y}\right)^2} \sqrt{1 + Dk_0^2 + \sqrt{4Dk_0^2 + 1}},
 \end{aligned}
 \tag{7.2}$$

where m and n are the numbers of half-waves of natural shape in the direction of the x - and y -axes:

$$k_0 = \sqrt{\left(\frac{m\pi}{L_x}\right)^2 + \left(\frac{n\pi}{L_y}\right)^2}.$$

Figure 13 illustrates the comparison of the boundaries calculated numerically (bold lines) and by the asymptotic formulas (7.2) (thin lines). Figure 13 *a* presents the flutter boundaries with respect to the third mode for $L_y = 1000, 200, 130, 110$, which are shown by solid, dashed, dash-dotted, and dotted lines, respectively. In Fig. 13 *b*, the same lines show the flutter boundaries with respect to the fourth mode for $L_y = 1000, 200, 100, 82$. One can see that an increase in the Mach numbers where the instability is observed in the “central” part of the flutter domain, $L_x = 100, \dots, 300$, is correctly described by the asymptotics. The difference is only in the region of small L_x , where the condition of large dimensions is not satisfied in the direction of the x -axis, and in the region of large M which is attained for sufficiently small L_y , where the condition of large dimensions of the plate is violated in the direction of the y -axis.

8. CONCLUSION

In the linear approximation, we study the stability problem for an elastic periodically supported strip with hinged front and back edges. One side of this strip is in the supersonic flow of a gas. The aerodynamics is described by the exact theory of potential flow of fluids, which holds for $M > 1$ including the region of small supersonic speeds. The flutter domains are numerically constructed for the first

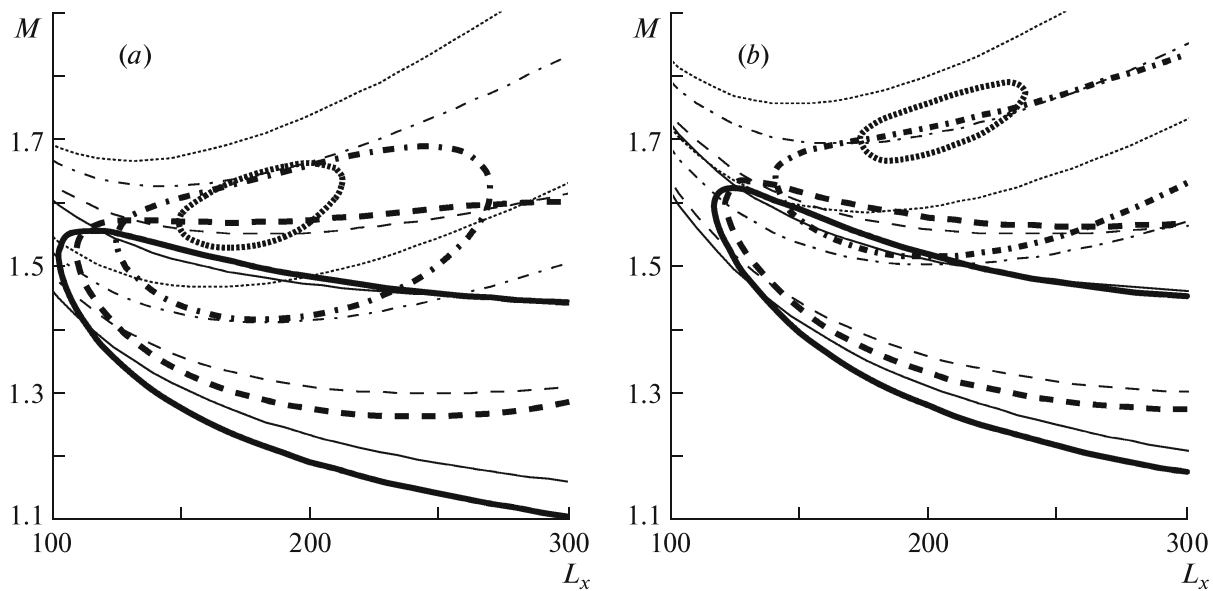


Fig. 13.

four eigenmodes. The flutter domain for the first mode consists of the coupled and single-mode flutter domains. The flutter domains for the other three modes are only the single-mode flutter domains.

For sufficiently large values of the span width L_y , the instability domains are close to the corresponding domains in the two-dimensional problem, which was solved in [25], where there is no dependence on the coordinate y . As the parameter L_y decreases, the instability domains change significantly. The instability domain for the first mode ceases to be simply connected and splits into two parts corresponding to single-mode and coupled flutter. As L_y continues to decrease, the single-mode flutter domain shrinks to a point and disappears; the coupled flutter domain continues to move towards higher values of L_x . For the other modes, the flutter domains also shrink and disappear, and the Mach numbers corresponding to instability also increase.

These results are compared with the results obtained by the piston theory, and it is shown that this theory does not permit discovering single-mode flutter, because its description of the aerodynamic problem is qualitatively false for small Mach numbers ($M < 1.7$). At the same time, the results of calculations by the exact and piston theories practically coincide for large M .

The results of calculations of single-mode flutter are comparable with the asymptotic theory, which qualitatively agrees with the calculations and explains the increase in the Mach number corresponding to the instability as L_y decreases.

ACKNOWLEDGMENTS

This research was supported by the Russian Foundation for Basic Research (grants Nos. 14-01-31547 and 14-01-00049) and by the Program of the President of the Russian Federation (grant No. MD-4544.2015.1).

REFERENCES

1. A. B. Movchan, "On Vibrations of a Plate Moving in a Gas," *Prikl. Mat. Mekh.* **20** (2), 211–222 (1956) [*J. Appl. Math. Mech. (Engl. Transl.)*].
2. A. B. Movchan, "On Stability of a Panel Moving in a Gas," *Prikl. Mat. Mekh.* **21** (2), 231–243 (1957) [*J. Appl. Math. Mech. (Engl. Transl.)*].
3. A. A. Il'yushin, "Law of Plane Sections in Supersonic High-Speed Aerodynamics," *Prikl. Mat. Mekh.* **20** (6), 733–755 (1956) [*J. Appl. Math. Mech. (Engl. Transl.)*].
4. V. V. Bolotin, *Nonconservative Problems of the Theory of Elastic Stability* (Fizmatgiz, Moscow, 1961; Pergamon Press, New York, 1963).
5. E. I. Grigolyuk, R. E. Lamper, and K. G. Shandarov, "Flutter of Panels and Shells," in *Progress in Science and Technology. Mechanics* (VINITI, Moscow, 1963), pp. 34–90 [in Russian].
6. J. Dugundji, "Theoretical Consideration of Panel Flutter at High Supersonic Mach Numbers," *AIAA J.* **4** (7), 1257–1266 (1966).

7. E. Y. Dowell, *Aeroelasticity of Plates and Shells* (Noordhoff International Publ., Leyden, 1974).
8. Yu. N. Novichkov, "Flutter of Plates and Shells," in *Progress in Science and Technology. Mechanics of Deformable Solids*, Vol. 11 (VINITI, Moscow, 1978), pp. 67–122 [in Russian].
9. C. Mei, K. Abdel-Motagaly, and R. R. Chen, "Review of Nonlinear Panel Flutter at Supersonic and Hypersonic Speeds," *Appl. Mech. Rev.* **10**, 321–332 (1999).
10. S. D. Algasin and I. A. Kiiko, *Flutter of Plates and Shells* (Nauka, Moscow, 2006) [in Russian].
11. I. A. Kiiko and V. V. Pokazeev, "Vibrations and Stability of a Viscoelastic Strip Placed into a Gas Flow," *Dokl. Ross. Akad. Nauk* **410** (3), 342–344 (2005) [*Dokl. Phys. (Engl. Transl.)* **50** (3), 158–160 (2005)].
12. B. Duan, K. Abdel-Motagaly, X. Guo, and C. Mei, "Suppression of Supersonic Panel Flutter and Thermal Deflection Using Shape Memory Alloy," *AIAA Paper*, AIAA-2003-1513 (2003).
13. R. C. Zhou, Z. Lai, D. Y. Xue, et al., "Suppression of Nonlinear Panel Flutter with Piezoelectric Actuation Using Finite Element Method," *AIAA J.* **33** (6), 1098–1105 (1995).
14. Dun Min-De, "On the Stability of Elastic Plates in a Supersonic Stream," *Dokl. Akad. Nauk SSSR* **120** (4), 726–729 (1958) [*Sov. Phys. Dokl. (Engl. Transl.)* **3**, 479–482 (1958)].
15. H. C. Nelson and H. J. Cunnigham, "Theoretical Investigation of Flutter of Two-Dimensional Flat Panels with One Surface Exposed to Supersonic Potential Flow," *NACA Report No.* 1280 (1956).
16. T. Y. Yang, "Flutter of Flat Finite Element Panels in Supersonic Potential Flow," *AIAA J.* **13** (11), 1502–1507 (1975) [*Raketen. Tekhn. Kosmonavt. (Russ. Transl.)* **13** (11), 110–117 (1975)].
17. O. O. Bendiksen and G. A. Davis, "Nonlinear Travelling Wave Flutter of Panels in Transonic Flow," *AIAA Paper*, AIAA-95-1486 (1995).
18. O. O. Bendiksen and G. Seber, "Fluid-Structure Interactions with Both Structural and Fluid Nonlinearities," *J. Sound Vibr.* **315** (3), 664–684 (2008).
19. E. H. Dowell, "Aerodynamic Boundary Layer Effect on Flutter and Damping of Plates," *J. Aircraft* **10** (12), 734–738 (1973).
20. R. P. Selvam, M. R. Visbal, and S. A. Morton, "Computation of Nonlinear Viscous Panel Flutter Using a Fully-Impact Aeroelastic Solver," *AIAA Paper*, AIAA-98-1844 (1998).
21. R. E. Gordnier and M. R. Visbal, "Computation of Three-Dimensional Nonlinear Panel Flutter," *AIAA Paper*, AIAA-2001-0571 (2001).
22. A. Hashimoto, T. Aoyama, and Y. Nakamura, "Effect of Turbulent Boundary Layer on Panel Flutter," *AIAA J.* **47** (12), 2785–2791 (2009).
23. V. V. Vedenev, "Flutter of a Wide Strip Plate in a Supersonic Gas Flow," *Izv. Akad. Nauk. Mekh. Zhidk. Gaza*, No. 5, 155–169 (2005) [*Mech. Fluids (Engl. Transl.)* **40** (5), 805–817 (2005)].
24. A. G. Kulikovskii, "On the Stability of Homogeneous States," *Prikl. Mat. Mekh.* **30** (1), 148–153 (1966) [*J. Appl. Math. Mech. (Engl. Transl.)* **30** (1), 180–187 (1966)].
25. V. V. Vedenev, "Panel Flutter at Low Supersonic Speeds," *J. Fluids Struct.* **19**, 79–96 (2012).
26. V. V. Vedenev, "Interaction of Panel Flutter with Inviscid Boundary Layer Instability in Supersonic Flow," *J. Fluid Mech.* **736**, 216–249 (2013).
27. V. V. Vedenev, "Effect of Damping on Flutter of Simply Supported and Clamped Panels at Low Supersonic Speeds," *J. Fluid Struct.* **40**, 366–372 (2013).
28. V. V. Vedenev, S. V. Guvernyuk, A. F. Zubkov, and M. E. Kolotnikov, "Experimental Investigation of Single-Mode Panel Flutter in Supersonic Gas Flow," *Izv. Akad. Nauk. Mekh. Zhidk. Gaza*, No. 2, 161–175 (2010) [*Mech. Fluids (Engl. Transl.)* **45** (2), 312–324 (2010)].
29. V. V. Vedenev, "Nonlinear High-Frequency Flutter of a Plate," *Izv. Akad. Nauk. Mekh. Zhidk. Gaza*, No. 5, 197–208 (2007) [*Mech. Fluids (Engl. Transl.)* **42** (5), 858–868 (2007)].
30. V. V. Vedenev, "Limit Oscillatory Cycles in the Single Mode Flutter of a Plate," *Prikl. Mat. Mekh.* **77** (3), 355–370 (2013) [*J. Appl. Math. Mech. (Engl. Transl.)* **77** (3), 257–267 (2013)].
31. V. V. Vedenev, "High-Frequency Flutter of a Rectangular Plate," *Izv. Akad. Nauk. Mekh. Zhidk. Gaza*, No. 4, 173–181 (2006) [*Mech. Fluids (Engl. Transl.)* **41** (4), 641–648 (2006)].
32. V. V. Vedenev, "Study of the Single-Mode Flutter of a Rectangular Plate in the Case of Variable Amplification of the Eigenmode along the Plate," *Izv. Akad. Nauk. Mekh. Zhidk. Gaza*, No. 4, 163–174 (2010) [*Mech. Fluids (Engl. Transl.)* **45** (4), 656–666 (2010)].
33. A. G. Kulikovskii, "The Global Instability of Uniform Flows in Non-One-Dimensional Regions," *Prikl. Mat. Mekh.* **70** (2), 257–263 (2006) [*J. Appl. Math. Mech. (Engl. Transl.)* **70** (2), 229–234 (2006)].
34. J. W. Miles, *The Potential Theory of Unsteady Supersonic Flow* (Cambridge Univ. Press, Cambridge, 1959; Fizmatgiz, Moscow, 1963).
35. S. I. Soloviev, "The Finite-Element Method for Symmetric Nonlinear Eigenvalue Problems," *Zh. Vychisl. Mat. Mat. Fiz.* **37** (11), 1311–1318 (1997) [*Comput. Math. Math. Phys. (Engl. Transl.)* **37** (11), 1269–1276 (1997)].
36. M. A. Lavrentiev and B. V. Shabat, *Method of the Theory of Functions of a Complex Variable* (Nauka, Moscow, 1973) [in Russian].